Optimization of an HTS Induction/Synchronous Motor According to Changing of HTS Tapes Critical Current by Analytical Hierarchy Process

F. Kazemzadeh[i][*] and H. Heydari[ii]

ABSTRACT

This paper represents the performance of a squirrel-cage High Temperature Superconducting Induction/ Synchronous Motor (HTS-ISM) based on nonlinear electrical equivalent circuit. The structure of the HTS-ISM is the same as that of the squirrel-cage type induction machine, and the secondary windings are fabricated by the use of the HTS wires. It has already been shown that based on the experiments that even this simple replacement realizes the excellent improvement of the performances such as coexistence of slip and synchronous rotations, higher efficiency (due to the synchronous operation), and robustness against the overload. In this paper, the transient modeling of this motor is performed by Matlab Simulink. Also, it is shown by FEM that starting and synchronous torque is extremely dependent on input voltage and critical current of superconducting tapes of the rotor. So, the starting and synchronous torque of the HTS induction motor can be improved with adjustment of the input voltage and critical current of the rotor HTS tapes. Also, in order to optimize both the starting and synchronous torques simultaneously, the relationship between these torques and the critical current of the HTS tapes have been investigated. Finally, according to the variation of the critical current, we optimized the design of the motor by analytical hierarchy process with finding the appropriate critical current for HTS tapes of rotor. The equations obtained are nonlinear, and then the typical Newton–Raphson method is used for the calculation.

KEYWORDS

HTS induction motor optimization, superconducting rotor, HTS-ISM, Analytical Hierarchy Process

1. INTRODUCTION

Squirrel-cage induction motors have been widely utilized as the conventional type, because of the simple structure, low cost, easy maintenance, availability of mass production, etc. The aforementioned merits are crucial from the point of view of practical applications, even though the energy conversion efficiency of this type of motor is generally not so high compared to that of synchronous counterparts. For instance, it is known that all inverter-fed motors in electric trains have been fabricated by means of the squirrel-cage-type induction motor in the world. Therefore, the target is the application of HTS tape conductors to such a motor in order to make a breakthrough for the rotating mechanism as well as the rotation control method of the motor. With respect to the aforementioned HTS induction motor, Sim

et al have already reported experimental results from using a rotor fabricated with Bi-2223/Ag tapes [1], [2], and shown that the synchronous torque has successfully been observed. To the authors' knowledge, these are the first direct reports of the coexistence of slippage and synchronous torques. Unfortunately, the theoretical discussions for the explanation of the tested results in their reports are inadequate, and more detailed tests are also necessary in order to clarify the rotating mechanism of the motor. Ishigohka et *al* have also reported experimental results for a similar type motor with fractional horse power [3]. Their group, unfortunately, has not yet succeeded in observing the synchronous torque, due to the problems of the HTS end rings. The group at Kyoto University also has been developing such that motor in several cases and they calls this motor an

---

i [*] Corresponding Author, F. Kazemzadeh is with the High Voltage and Magnetic Material Research Center, Electrical Engineering Department, Iran University of Science and Technology (IUST), Tehran 1684613114, Iran (e-mail: fkazemzadeh@elec.iust.ac.ir).

ii H. Heydari is with the Center of Excellence for Power System Automation and Operation, Iran University of Science and Technology (IUST), Tehran 1684613114, Iran (e-mail: heydari@iust.ac.ir).

'HTS induction/synchronous motor: HTS-ISM', because such a motor has both slippage and synchronous modes: even the structure of this motor is the same as that of the squirrel-cage type [4]–[8]. This group also reported the rotating mechanism of the Aforementioned HTS induction motor based upon the electrical equivalent circuit, in which the nonlinear current transport properties are taken into account [9], [10]. They have already shown, based on analysis and experiment, that simple replacement of the secondary windings with Bi-2223 multifilamentary tapes realizes exciting characteristics, such as co-existence of slip and synchronous rotation, almost constant torque versus speed curve, etc.

In the theory, the motor starts rotating when the HTS secondary windings transit from a zero resistivity state to a flux-flow state (not a normal conducting state). The rotating speed increases at the slip mode by increasing the input voltage, and then the motor is finally pulled in (synchronous speed), by trapping the interlinked magnetic fluxes in the secondary windings. This mechanism indicates the really important point that the simple replacement of the squirrel-cage windings with HTS conductors results in the possession of both of asynchronous and synchronous torques. These characteristics are impossible to obtain in the case of any conventional (normal conducting) motor. It should be noted that our subject motor is still categorized as an induction motor, even though it has the above-mentioned synchronous mode; for example, the armature reaction is considered not to have occurred in this motor. In other words, the motor is an ultimate induction motor, as that has zero resistivity secondary windings. Further, the rotating process, i.e., 'starting' → 'acceleration' → 'synchronism', can automatically be realized with the aid of nonlinear current density versus electric field relations, i.e., so-called automatic secondary resistance control.

In this paper the performances of this motor were analyzed by means of the theoretical and numerical methods based on the electrical equivalent circuit. A wide range of electric field versus current density in HTS film is formulated based on the Weibull function, and analyzed as a non-linear resistance in the equivalent circuit. The equations obtained are nonlinear, and then the typical Newton–Raphson method is used for the calculation. The theoretical results are compared with experimental one. The transient state of this HTS induction motor is modeled by Matlab Simulink. Also it is shown by FEM that starting and synchronous torque extremely is dependent to input voltage and critical current of superconducting tapes of rotor and so the starting and synchronous torque of the HTS induction motor can be improved with adjustment of critical current of rotor HTS tapes. Furthermore, large synchronous torque can also be realized by trapping the magnetic flux in the rotor circuit because of the persistent current mode.

Also, the relation of starting and synchronous torque with changes of the critical current of the HTS tapes to optimization of these two torques have been investigated with numerical methods and according to variation of the critical current we optimized the designing of the motor by analytical hierarchy process with finding the appropriate critical current for HTS tapes of rotor.

2. STRUCTURE OF THE HTS-ISM

A commercialized squirrel-cage induction motor, three-phase, four-pole, 1.5 kW class at room temperature, is considered in this paper. The number of turns of the primary windings is 264. The number of slots in the stator and the rotor is, respectively, 36 and 44.

Only the secondary windings of the above-mentioned motor were replaced with the superconducting tapes. The rotor bars and end rings were separately prepared, and then soldered together. Table I lists the HTS-ISM parameters in the considered model.

TABLE I
HTS-ISM parameters in the simulation model

Symbol	Quantity	Value
P	Nominal power (kW)	1.5
V_l	Voltage (V)	200
L	Motor length (m)	0.15
D	Motor diameter (m)	0.175
g	Air gap length (mm)	0.5
T_s	Turn number of stator winding	270
p	Pole number	4
S_s	Number of stator slots	36
S_r	Number of rotor slots	44
R_s	Phase-resistance of stator winding (Ω)	0.12
X_s	Phase-reactance of stator winding (Ω)	1.82
X_r	Phase-reactance of stator winding (Ω)	1.82
X_M	Mutual phase-reactance (Ω)	45
R_c	Phase-core loss resistance	275
a_{sr}	Conversion ratio of stator to rotor	26.7

Table II lists the specifications of the DI-BSCCO tapes for the squirrel-cage rotor windings [4]. It is used different kinds of tapes for the rotor bars and end rings. That is, the width of the tape for the rotor bars is narrower than that for the end rings. This is because the slot width of the rotor core is less than 3.3 mm (the width is dependent on the radial direction of the rotor). In contrast, there are no spatial limitations for the end rings, and the wider width, i.e. larger critical current, DI-BSCCO tapes are utilized in order to always be in the superconducting (zero resistivity) state. Then, the nominal critical currents of the tapes are, respectively, 63 A and 138 A, at 77 K and self-field.

TABLE II
Specifications of DI-BSCCO tapes

Symbol	Rotor bar	End ring
Width (mm)	2.6	4.1
Thickness (mm)	0.18	0.21
Nominal critical current (A)	63	138

Fig. 1 illustrates the schematic diagram of the cross section of a rotor slot. As can be seen, the superconducting rotor bar is put at the outermost surface of the rotor, i.e., near the air-gap, in order to reduce the effect of the leakage magnetic flux [5].
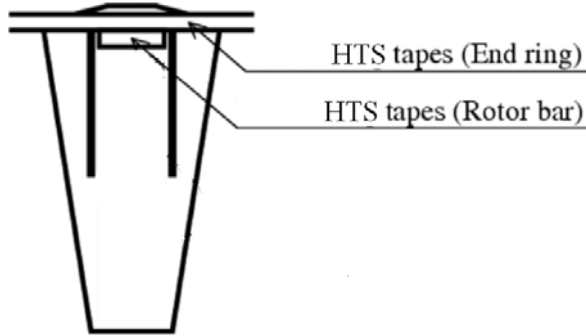

Figure 1: Schematic diagram of a rotor with rotor bar and end ring

As the iron core absorbs almost all of the main magnetic flux from the slot, the use of such a rotor core brings about two advantages compared to a machine without the core. Firstly, there is only a self magnetic field in the slots, i.e., magnetic field leakage from the current flowing in HTS bars. In other words, there is no external magnetic field in them, so the detrimental effect of the magnetic field on the current transport property in superconducting HTS can be avoided. Furthermore, the flux creep induced in the HTS does not need to be taken into account. Secondly, the reductions of the electromagnetic force acting on the HTS conductors. Therefore, we do not need to consider the complicated structure supporting the HTS conductors [9].

3. DYNAMICAL MODELING OF THE HTS-ISM

In order to analysis with the use of the electrical equivalent circuit, the nonlinear current transport property has to be formulated. The following power-law expression is widely utilized for the approximate formulation of the flux-flow state. [10], [11]:

$$E = E_c \left(\frac{i}{i_c(B,T)} \right)^{n(B,T)} \tag{1}$$

$$i_c(B,T) = \frac{i_{C0}}{1 + B/B_0} \times \frac{1 - T/T_c}{1 - T_0/T_c} \tag{2}$$

$$n(B,T) = \left(n_1 + \frac{n_0 - n_1}{1 + B/B_0} \right) \times \frac{T_0}{T} \tag{3}$$

Where, Eo denotes the electric field criterion for the definition of the critical current (Ic). The typical value of Eo is 0.1 μV/cm or 1 μV/cm. The power law index n is

called n-value, and shows the steepness of the take-off of the E-I curve. It should be noted that higher n-value is important for the realization of the constant torque vs. slip curve. The value of n for the curve of Fig. 2 is 4.
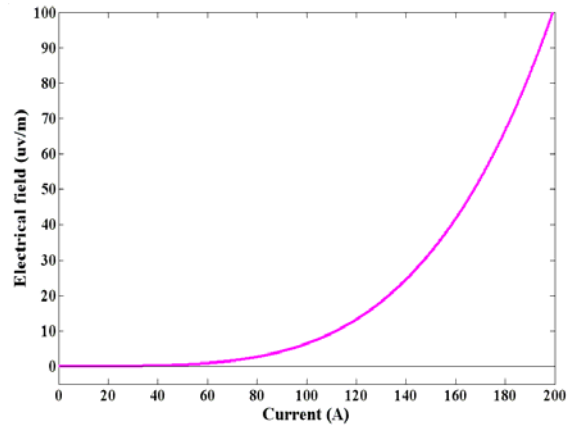

Figure 2: Typical curve of electric field *(E)* vs. current *(I)* property at 77 K and self-field in Bi-2223/Ag multifilament tape utilized for the rotor bars. The tape shows zero resistivity until the current reaches about 63A (critical current).

Therefore, unlike conventional induction motors with a fixed secondary resistance at all current and rotor speeds, the secondary resistance of HTS induction motor will change in each current flowing through the superconducting tapes of rotor. In fact for each current and speed of the motor, there will be a specific secondary resistance. Fig .3(a) demonstrates equivalent circuit of slip mode that the secondary resistance is changeable. On the other hand, when the above-mentioned resistance becomes zero by accelerating, i.e., the corresponding slip frequency reduces; the persistent current mode will be realized. in that case the interlinked magnetic fluxes will be trapped in the windings, and then the voltage source, V'$_{2s}$,equivalently appears at the secondary windings, i.e., synchronous mode (Fig.3(b)) [4].
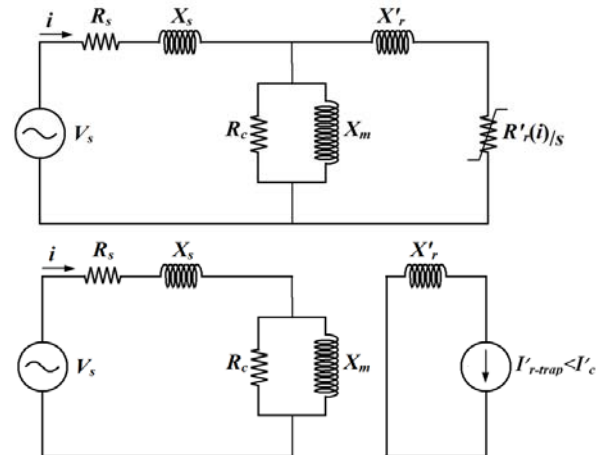

Figure 3: Electrical equivalent circuit of HTS induction motor for one phase. (a)slip mode (flux flow); (b)synchronous mode.

In order to obtain the changes in torque, speed, current and resistance of superconducting tapes during the starting and achieving to steady state mode of induction motor, Matlab Simulink can be used. Thus, the procedure is first obtain the voltages of the q and d axis by using Park convertor., followed by the flux and current of q and d axis is obtained and ultimately we can obtain dynamic curves of torque and speed of HTS induction motor. Note that here there is that unlike a conventional squirrel cage induction motors with constant rotor resistance, the resistance of superconducting rotor of HTS induction motor was variable and depends on the current changes induced by the stator flux. So the HTS power law can be applied in the modeling of superconductor tapes, and the resistance changes of superconducting rotor tapes during the simulation process and the effects of this variable resistance on torque, speed and current of the HTS induction motor was investigated.

Parameters used in the dynamical simulation of this motor are given by the following relations.

The voltages of each phase are given by:

$$v_a = v_m \cos(2\pi ft) \tag{4}$$

$$v_b = v_m \cos(2\pi ft - \frac{2\pi}{3}) \tag{5}$$

$$v_c = v_m \cos(2\pi ft + \frac{2\pi}{3}) \tag{6}$$

The voltages of q-axes and d-axes are given by:

$$v_{qs} = \frac{1}{3}(2v_a - v_b - v_c) \tag{7}$$

$$v_{ds} = \frac{1}{\sqrt{3}}(v_c - v_b) \tag{8}$$

The fluxes of q-axes and d-axes of stator and rotor and also mutual flux of them are given by:

$$\psi_{qs} = \omega_b \int \left[v_{qs} + \frac{r_s}{x_{ls}}(\psi_{qm} - \psi_{qs}) \right] dt \tag{9}$$

$$\psi_{ds} = \omega_b \int \left[v_{ds} + \frac{r_s}{x_{ls}}(\psi_{dm} - \psi_{ds}) \right] dt \tag{10}$$

$$\psi'_{qr} = \omega_b \int \left[v'_{qr} - \omega_r \psi'_{dr} + r'_r (\psi_{qm} - \psi'_{qr}) \right] dt \tag{11}$$

$$\psi'_{dr} = \omega_b \int \left[v'_{dr} + \omega_r \psi'_{qr} + r'_r (\psi_{dm} - \psi'_{dr}) \right] dt \tag{12}$$

$$\psi_{qm} = x_M \left(\frac{\psi_{qs}}{x_{ls}} + \frac{\psi'_{qr}}{x'_{lr}} \right) \tag{13}$$

$$\psi_{dm} = x_M \left(\frac{\psi_{ds}}{x_{ls}} + \frac{\psi'_{dr}}{x'_{lr}} \right) \tag{14}$$

$$\frac{1}{x_M} = \left[\frac{1}{x_m} + \frac{1}{x_{ls}} + \frac{1}{x'_{lr}} \right] \tag{15}$$

The resistance of superconducting rotor is variable and it depends on induced current from stator rotational flux to rotor superconducting tapes, so its relation is given by:

$$r'_r = \frac{1}{3} \frac{a_{sr}^2 s_r l_r E_c \left(\frac{a_{sr} i'_r}{i_c} \right)^n}{a_{sr} i'_r} \tag{16}$$

The currents of q-axes and d-axes of stator and rotor given by:

$$i_{qs} = \frac{\psi_{qs} - \psi_{qm}}{x_{ls}} \tag{17}$$

$$i_{ds} = \frac{\psi_{ds} - \psi_{dm}}{x_{ls}} \tag{18}$$

$$i'_{qr} = \frac{\psi'_{qr} - \psi_{qm}}{x'_{lr}} \tag{19}$$

$$i'_{dr} = \frac{\psi'_{dr} - \psi_{dm}}{x'_{lr}} \tag{20}$$

Therefore, the stator and rotor currents for each phase are as follows:

$$i_{as} = i_{qs} \tag{21}$$

$$i_{bs} = -\frac{1}{2}(i_{qs} + \sqrt{3}i_{ds}) \tag{22}$$

$$i_{cs} = -\frac{1}{2}(i_{qs} - \sqrt{3}i_{ds}) \tag{23}$$

$$i'_{ar} = i'_{qr} \tag{24}$$

$$i'_{br} = -\frac{1}{2}(i'_{qr} + \sqrt{3}i'_{dr}) \tag{25}$$

$$i'_{cr} = -\frac{1}{2}(i'_{qr} - \sqrt{3}i'_{dr}) \tag{26}$$

So at the end the induced electrical torque and rotor speed are obtained as follows:

$$T_e = \frac{3}{2}\left(\frac{p}{2}\right)\frac{1}{\omega_b}\left[\psi_{ds} i_{qs} - \psi_{qs} i_{ds} \right] \tag{27}$$

$$\omega_r = \frac{1}{J} \int (T_e - T_{mec} - T_f) dt \tag{28}$$

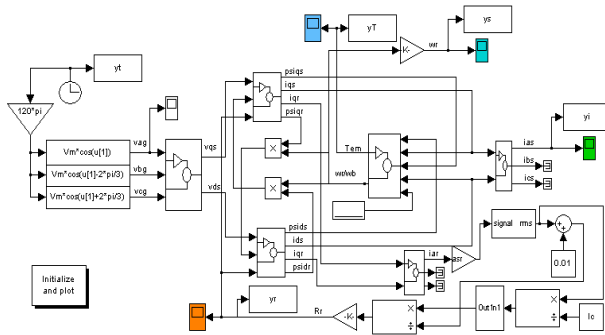By applying above equations in Matlab Simulink, diagram of Fig. 4 can be produced.

Figure 4: Dynamical model of The HTS-ISM in Matlab Simulink

Figure 8: Superconducting rotor resistance was transferred to the stator side

The applied load torque is equal to 9Nm. By running above program for the duration of 2s from starting to reaching the steady state mode can obtain any of the output electrical torque curve, motor speed, stator current and resistance of the superconductive rotor respectively in Figures 5, 6, 7 and 8. In the Fig. 6, program running is continued to 10 s and the final speed is stabled in 1799.3 rpm. The slip equivalent of that is 0.0004.
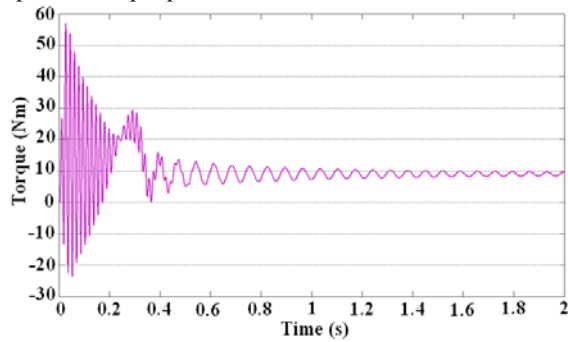
Figure 5: Dynamical torque of The HTS-ISM
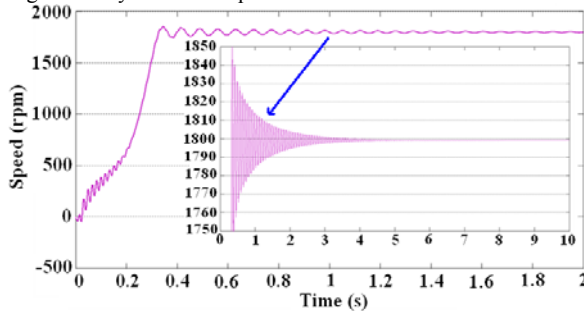
Figure 6: Dynamical speed of The HTS-ISM
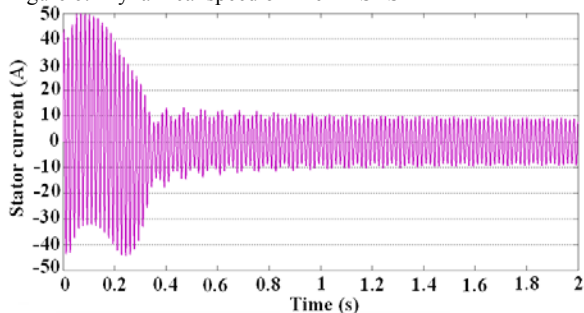
Figure 7: Stator current of The HTS-ISM

Fig. 5 shows the motor electrical torque. Damping Torque intended for the motor is zero. The applied mechanical load torque is equal to Nm 6 so the electric torque produced in the motor at the steady state is equal to 6 Nm. Fig. 6 shows the motor speed curves that as it is clear despite of sufficient mechanical load, the motor could ultimately increase its speed to synchronous speed. Fig. 7 shows the current drawn from the source that the balance of the current at the starting moment and also in steady state mode of motor is clear. Fig. 8 shows the superconducting rotor resistance variation that from the value of 6 ohms at the starting moment to value of zero at the steady state mode has decreased.

4. GENERATION CONDITIONS OF STARTING TORQUE FOR THE HTS-ISM

In a three-phase squirrel-cage induction motor the rotating stator field B_S induces a voltage in the rotor bars. The rotor voltage produces a rotor current follow, which lags by θ_r behind the voltage because of the inductance of the rotor.

$$(\theta_r = tg^{-1}\frac{X_r}{R_r})$$ (29)

The X_r and R_r denote the leakage reactance and ohmic resistance of the rotor respectively. The rotor current produces a rotor magnetic field B_R lagging 90° behind itself, and B_R interacts with B_S to produce a torque in the machine. The induced Torque in the motor is given by:

$$\tau_{ind} = k\, B_r\, B_s\, \sin(\pi/2 + \theta_r)$$ (30)

While the rotor bars are in the superconductivity state, the resistance of the rotor is very low and θ_r is around 90°. So the induced torque in the motor would be approximately zero. Then as long as the superconductivity tapes are in the non-resistant state, there will be no starting torque at the motor and in no way the motor will start. If the critical current of HTS tape be high, in this case the induced current can't remove the HTS tapes from superconductivity to flux flow state. So for critical current of 189A, the distribution of the flux density in the rotor at the 0.01s and 0.1s of starting time are shown in Figs. 9 and 10. As it is clear at this state the rotor acts as a field shielding.
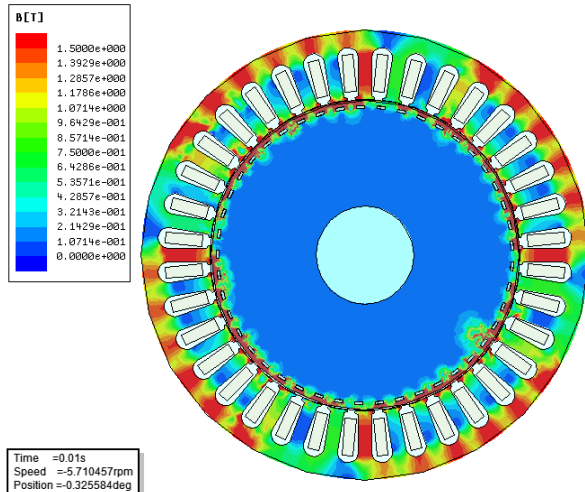
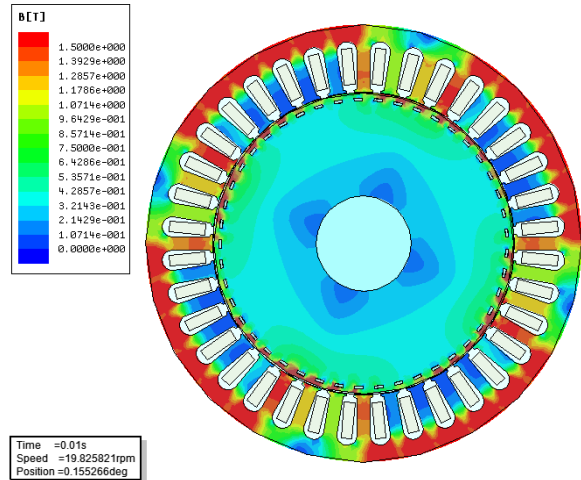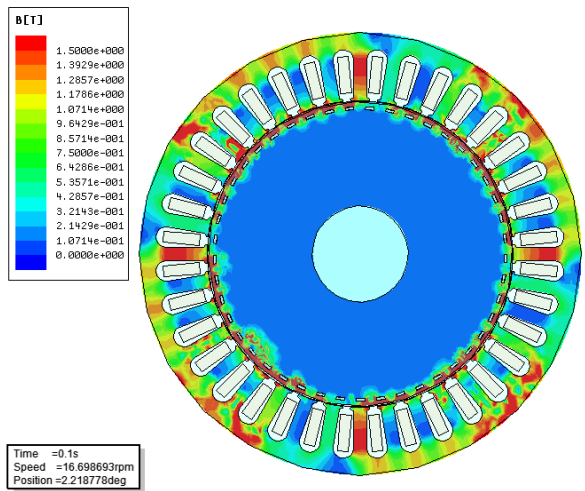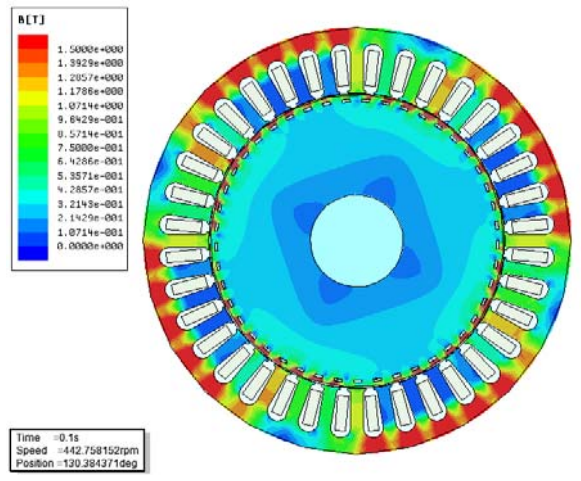Figure 9: Distribution of flux density for the critical current of 189A at t=0.01s.

Figure 10: Distribution of flux density for the critical current of 189A at t=0.1s.

This mode continues until the total currents induced at the HTS tapes are less than the critical current. But when the critical current is low enough, so the induced current passing from any HTS bars reaches its critical value, HTS tapes will go to flux-flow state (mixed state) and will undergo some resistance. The resistance of the superconducting tapes will not be zero by going to flux flow state; and by the increase of this resistance, the motors' capacity to create the necessary torque will be launched. So for critical current of 63A, the distribution of the flux density in the rotor at the 0.01s and 0.1s of starting time are shown in Figs. 11 and 12. As it is clear at this state the rotor can start itself.

Figure 11: Distribution of flux density for the critical current of 63A at t=0.01s.

Figure 12: Distribution of flux density for the critical current of 63A at t=0.1s.

As it is clear in this case the motor has been able to starting and increasing its speed to 442.7rpm after 0.1s. In this time the motor has rotated 130°.

5. APPEARING THE SYNCHRONOUS TORQUE IN THE HTS-ISM

The HTS-ISM is simulated by FEM. The no-load speed of motor from starting to reach the stable speed is shown in Fig. 13. The considered frequency in the FEM design is 50 Hz.
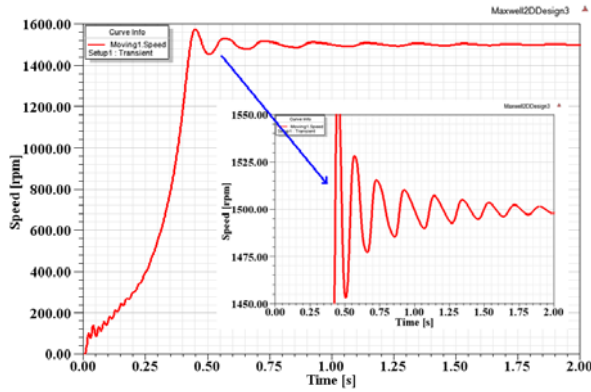
Figure 13: No-load speed of motor from starting to reach the synchronous speed

Figure 15: Persistent current density in an HTS bare of rotor at the synchronous speed

As it is clear the motor started hardly and at the end has reached to synchronous speed. The synchronous speed obtained for two reasons. Firstly the rotor resistance of rotor at the stable state is very slow. So in this case the nominal speed will be very larger. Secondly at the high speed the induced current to the rotor HRS tapes is slow, so at the passing state of the rotor from flux-flow state (having resistance) to superconducting state (no resistance) can create persistent current in the rotor loops. So the field trapped in the rotor can provide the synchronous speed to motor. Since, the rotor resistance is not absolute zero, so the persistent current is temporarily. The time constant is calculated by:

$$\tau = \frac{L_r}{R_r} \qquad (31)$$

The distribution of flux density at the synchronous speed is shown in Fig. 14.
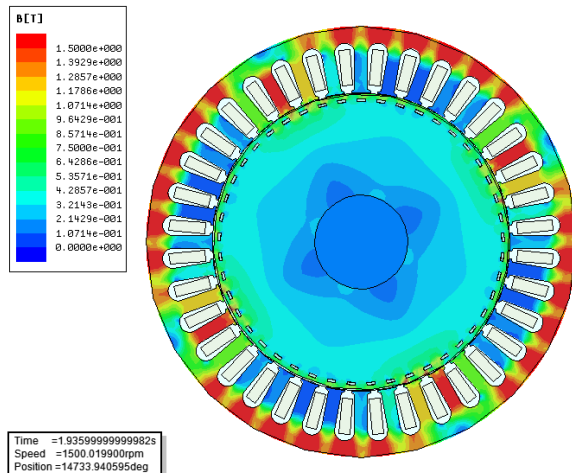

Figure 14: The distribution of flux density at the synchronous speed

The persistent current in an HTS bare of rotor at the synchronous speed is shown in Fig. 15.
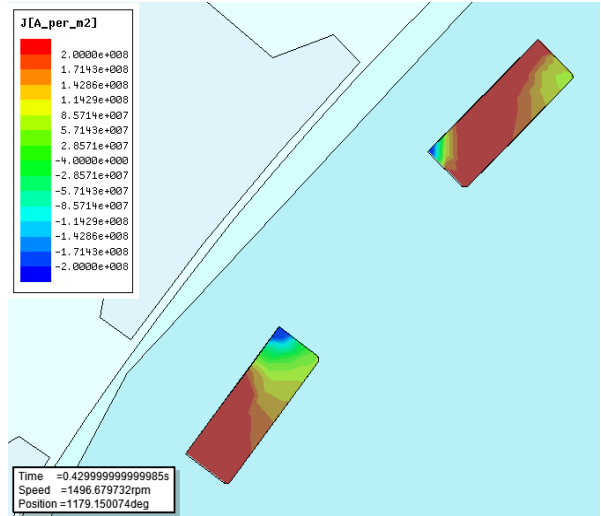
6. STATIC MODELING OF THE HTS-ISM

To optimization of the HTS-ISM, it is necessary to modeling of the operation characteristics of the motor in static state. So in this part the process of this modeling is described

The non-linear equation of resistance for the HTS rotor in each phase transferred to the stator side can be expressed as follows:

$$r_r'(i_r') = \frac{1}{3}a_{sr}^2 \frac{lE_c \left(\frac{a_{sr}i_r'}{i_c}\right)^n}{a_{sr}i_r'} s_r \qquad (32)$$

The current of superconductivity nonlinear resistance is expressed as follows:

$$i_r' = \frac{Vs\varphi}{\sqrt{\left(x_{ls} + x_{lr}'\right)^2 + \left(r_s + \frac{r_r'(i_r')}{s}\right)^2}} \qquad (33)$$

In fact because of that the current and rotor resistance are independent to each other, to obtain the current and rotor curves, we should solve equations (32) and (33) for all of the s values from 1 to 0 with the step iteration at 10^{-3}.

On the other hand the induced rotor voltage on the stator versus current changes can be calculated according to motor speed as follows:

$$E = \frac{F(i_r')}{s} = \frac{r_r'(i_r')}{s}i_r' \qquad (34)$$

This induced voltage also can be calculated with the following equation.

$$E = \sqrt{\left(Vs\varphi\right)^2 - \left(x_{ls} + x'_{lr}\right)^2 \left(i'_r\right)^2 - r_s i'_r}$$

(35)

In this case, the output power is as follows:

$$P_o = 3Ei'_r = 3\frac{r'_r(i'_r)}{s}\left(i'_r\right)^2$$

(36)

Finally, the torque induced to superconductivity rotor can be modeled in the following.

$$T_e = \frac{pP_o}{2\omega_b}$$

(37)

Where the p is the number of poles and ω is angular velocity of frequency of power supply.

A. Minimum starting voltage of the HTS-ISM

In the experimental results it is shown that a minimum starting primary voltage is necessary to transit the HTS secondary windings from the zero resistivity state to a flux-flow state to obtain the ability for starting the motor [4]. Here we obtained the results by applying above equations in an algorithm. The flow chart of the algorithm used for calculating the minimum starting voltage is reported in Fig.16. The equations obtained are nonlinear, and then the typical Newton–Raphson method is used for the calculation. The comparison between analysis result and experimental one corroborates our results
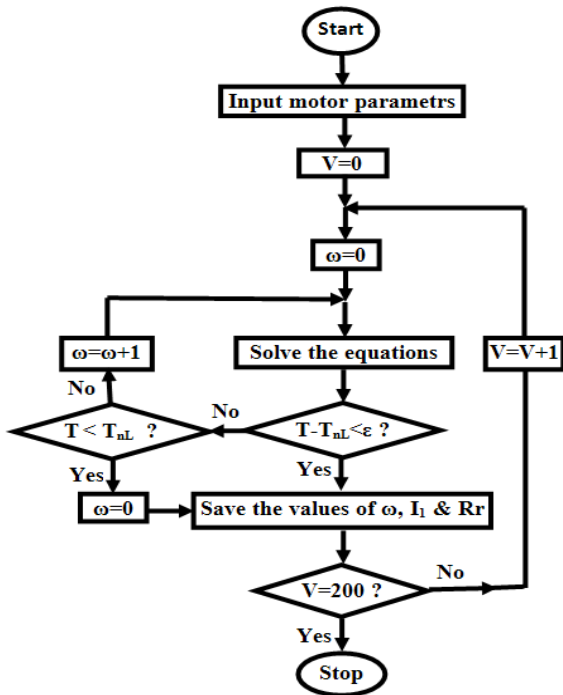

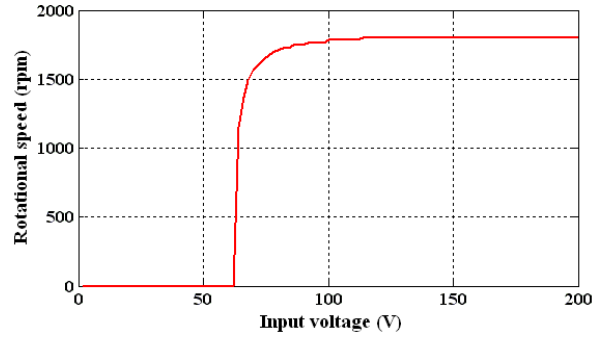Figure 16: Flow chart of the algorithm used for finding the minimum starting voltage for HTS-ISM.

Figure 17: Rotating speed (N) versus input voltage (V1) curves
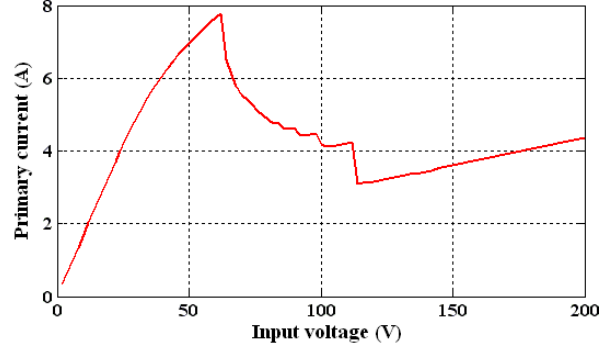

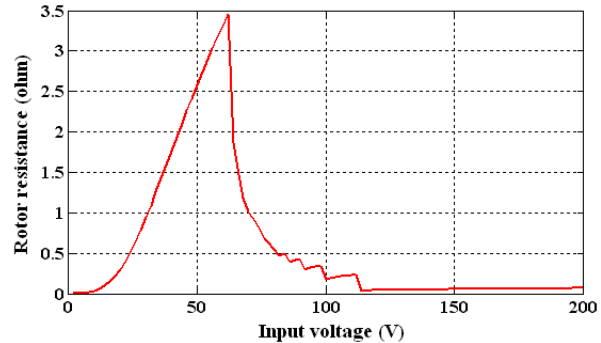Figure 28: Primary current (I1) versus input voltage (V1) curves

Figure 19: Rotor resistance (r'2) versus input voltage (V1) curves

Fig.17. shows analytical results of the rotating speed (N) versus input voltage (V1) curves and in the no-load condition. All results were carried out under the condition that the motor was in a steady state. As can be seen, the motor does not start rotating when the input voltage is low enough. This is because the rotating magnetic fluxes supplied from the three-phase primary windings Φ'_2, are shielded from the HTS rotor windings, due to the superconducting (dissipation less) shielding current. That is, the following relation (Kirchhoff's voltage law) is validated by the condition that the resistance of the secondary windings is zero. In this case, the torque is not generated due to $F'(I'_2)=0$ in Fig.17. In order to generate the starting torque, the magnetic fluxes must interlink the HTS squirrel-cage windings. This condition can be realized when the shielding current overcomes the HTS rotor bar's critical current, at which

the rotor bars are in the flux-flow (dissipative) state. It has been called the threshold voltage for entering this state the minimum starting voltage, V_{min} [7].

B. Torque characteristics for different critical currents

With the changes of critical current of HTS tapes, we can get different torque versus slip curve characteristics for motor. The characteristic curve of output torque, stator current and rotor resistance versus slip for different currents is obtained by above equations as Figs.20, 21, 22 respectively. The parameters derived are calculated for different slip, s. The slip is changed from 1 to 0 with the step iteration at 10^{-3}.

As it is clear, by increasing the critical current, the starting torque is reduced. But the input current of motor is increased (Fig.21) and also its resistance is decreased (Fig. 22).
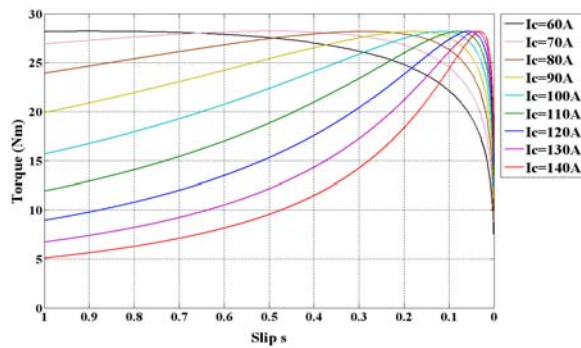

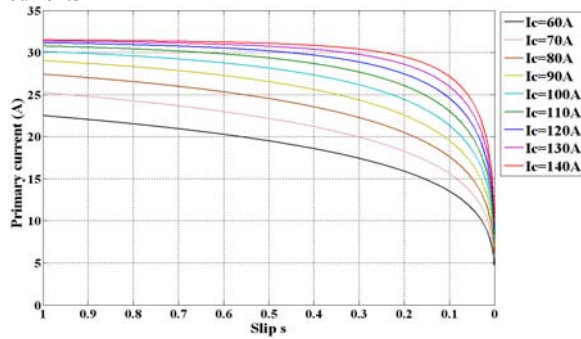Figure 20: Torque curve changes vs. slip for different critical currents

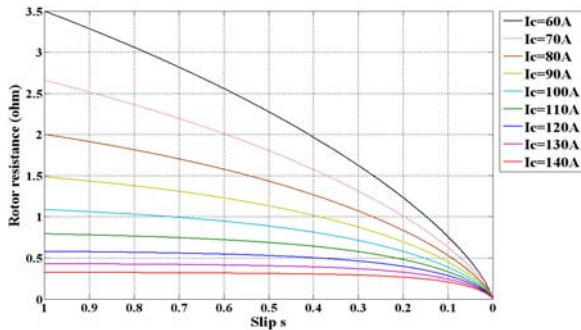Figure 21: Input current changes vs. slip for different critical currents

Figure 22: Resistance curve changes vs. slip converted into the primary side for different critical currents.

But for the synchronous mode, with increasing the critical current, unlike starting torque, the synchronous torque is increased. The reason is that with increasing the critical current, rotor bars regain their superconductivity at higher current (Fig.21) and torque (Fig.20) and so the synchronous torque in this current will be higher. Rotor resistance will be zero at synchronous mode (Fig.22).

7. DEPENDENCE OF THE STARTING AND SYNCHRONOUS TORQUES TO CRITICAL CURRENT

To obtain the starting torque diagram according to the critical current changes, we can use the above equations by placing slip value s = 1 and numerical solving the equations, achieve this curve in Fig.24 that is shown in blue. Red curve shows the synchronous torque that is obtained by detecting point to point of the amount of slip in which the tape current is reached the critical current of itself and the changes of equivalent torque for this slip of the critical currents have been achieved. The flow chart of the algorithm used for calculating the synchronous torque is reported in Fig.23.
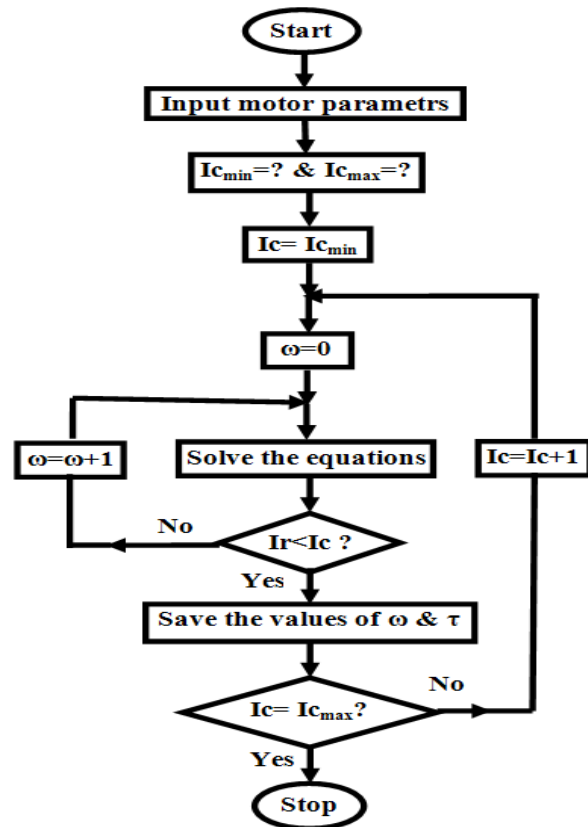

Figure 23: Flow chart of the algorithm used for calculating the synchronous torque
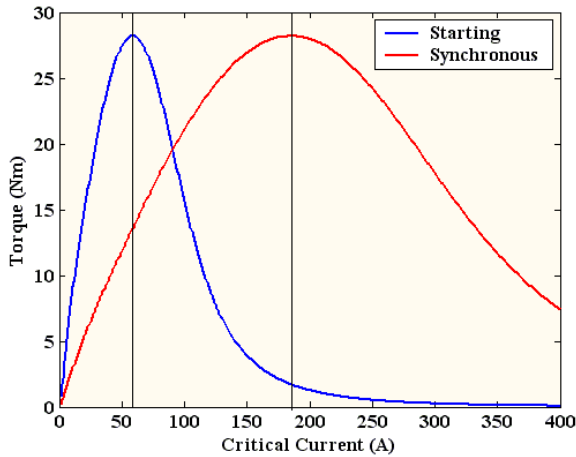
Figure 24: Starting and synchronous torque curves vs. changes of critical current

The reason of that the starting and synchronous torques any way do not exceed from 28 Nm is that Because that the maximum amount of torque that has obtained by a specified primary current of motor will not exceed that maximum torque according to the following optimization equations:

$$V_r^{'} = \sqrt{V_s^2 - (\omega(l_s + l_r^{'})I_r^{'})^2} - r_s I_r^{'} \tag{38}$$

$$\tau_{ind} = \frac{3pV_r^{'}I_r^{'}}{2\omega} \tag{39}$$

With placing (38) at (39) the output torque curve according to changes of primary input current is achieved in Fig.25. It is clear that the maximum amount of induction torque T_e=28Nm is obtained for $I_r^{'}$=22A.
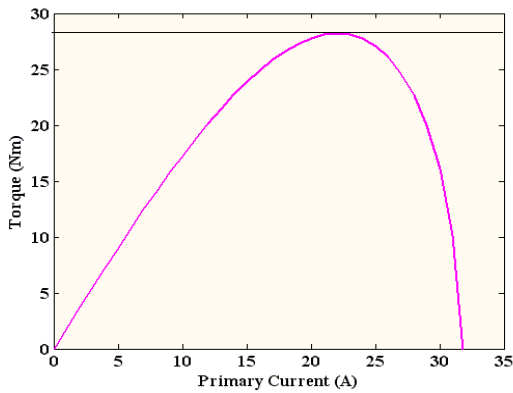

Figure 25: Induced torque curve vs. primary current changes

Fig. 24 can be divided into three regions. The first area (Ic=0-60) where starting and synchronizing torques both increased with increasing critical current. This area certainly can not be a good area to select the optimum critical current for HTS tapes because purpose of optimization is to finding the maximum value for booth the starting and synchronous torques and only the terminal point of this area (Ic =60) is most appropriate for

this region. The third area (Ic ≥180) also can not be an optimal area for starting and synchronous torque for this motor, Because in this area, both starting and synchronous torque curves reduce with increasing the critical current and the most appropriate for this area will be elementary point of this area (Ic=180). So the most appropriate area for selecting the critical current is the second area. In this area by increasing the critical current of HTS tapes the starting torque reduces but synchronous torque increases Therefore, the critical current selection in this area depends on HTS induction motor design condition. In this case if a high starting torque is needed, so the elementary points of this area would be suitable. But if you need to design with a high synchronous torque, then the end parts of this area will be suitable certainly. Of course, it is clear that more synchronous torque can be so important for our designing in HTS induction motors, so we can select the critical current during the end parts of this area and due to low starting torque of the motor firstly the motor start without load and at the synchronous state the load can be applied to the motor.

8. OPTIMIZATION OF THE HTS-ISM

So far the starting and synchronous torque curves depending on changes of the HTS tapes critical current of rotor was investigated. Two other important parameters that severally affect the design of the HTS induction motor are:

- HTS tapes cooling loss
- HTS tapes volume

Here optimization process of superconducting induction motor based on changes in the HTS tapes critical current is represented.

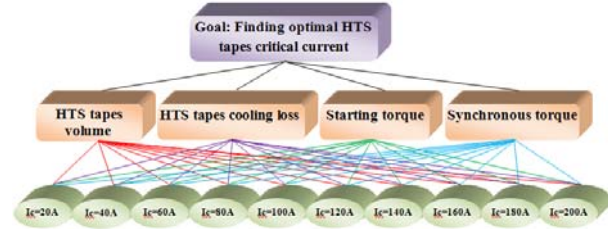*A. AHP Structure and Formulation*

Figure 26: Hierarchy process for optimal scheme.

The first step of the AHP (Analytical Hierarchy Process) is to structure the problem into graphical module comprising goal (optimal critical current), criteria, and alternatives (the 10 points of critical currents). Fig. 26 shows the structure of the winding scheme selection. Iterating from top to bottom, it contains optimal critical current at first level, criteria (four evaluation parameters) at the second level, and alternative ratings at the end.

Here the alternative ratings are the points of critical current points that divide the critical current to 10 sections.

Using the curves of synchronous torque and starting torque in Fig. 24, the weight values relative to these criterions are achieved.

As previously expressed in HTS induction/synchronous motors, during the starting moment that the induced current is high launched during induction is high which cause to the HTS tapes go from superconducting state with no resistance passing outside to flux flow state having resistance loss. in the way of stage operation If the induced current be increased high enough that even cause the HTS tapes may go to quench state with higher resistance., and increase the HTS ohmic losses caused due to more warming of HTS tapes. This causes that ultimately will make impossible to control temperature of HTS tapes and the tapes will cause damage. So we can consider the cooling loss as starting torque curve. The weight values relative to HTS tapes cooling loss criterion is achieved by inversing the starting torque criterion. HTS tapes volume can be appropriate to increase the critical current and the number of HTS tapes and considered linearly and so relative to HTS tapes volume criterion these weight values are related to value of critical current. The weight values for each alternative relative to each criterion are achieved through computer calculation with the help of expert choice (EC).

The weight of critical currents due to synchronous torque, starting torque, HTS tapes cooling loss, and HTS tapes volume are shown in Figs. 27–30, respectively. Considering Fig. 27, the Ic=180A has the largest weight; and in Fig. 28, the Ic=60A has the largest weight. From Fig. 29, the Ic=200A has the largest weight. From Fig. 30, the Ic=20A has the largest weight, and it can be seen that in all of the figures the rate of inconsistency is equal to 0.

The weight of criteria is shown in Fig. 31. It can be seen that the rate of inconsistency is 0.00776 and the starting torque has the largest weight. The final weight of the proposed critical current values calculated by EC is shown in Fig. 32. It can be seen that the Ic=60A has the largest weight, whereas the Ic=80A, Ic=40A, Ic=100A, Ic=120A, and…, have lower weight, respectively. This result confirms the critical current of 63A that have been selected by Kyoto University group in designing of the HTS-ISM in reference [4].
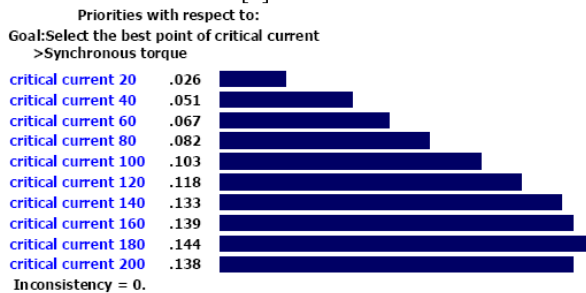

Figure 27: Weights of critical currents due to synchronous torque
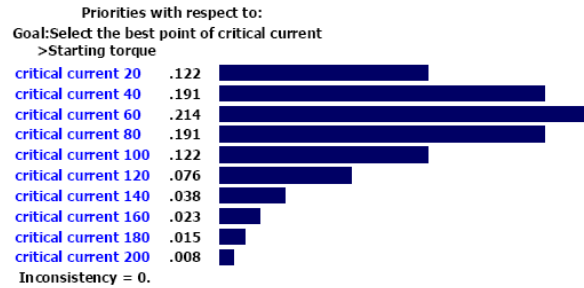

Figure 28: Weights of critical currents due to starting torque
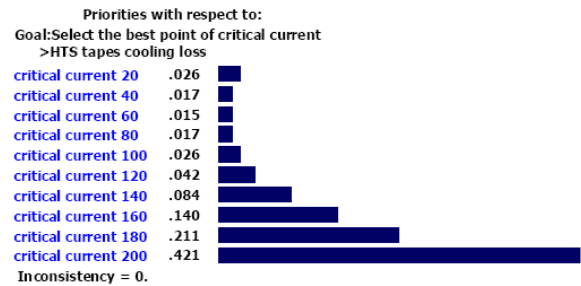

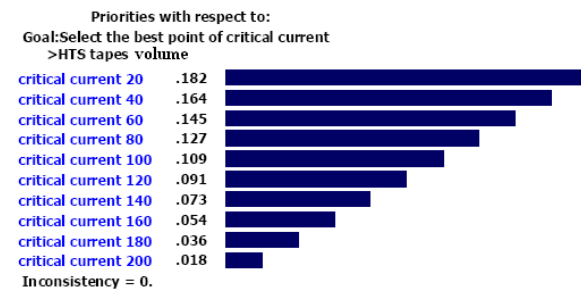Figure 29: Weights of critical currents due to HTS tapes cooling loss

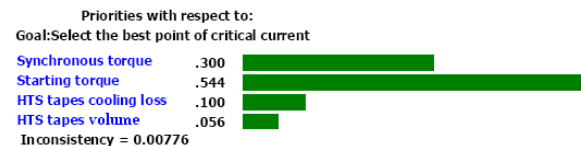Figure 30: Weights of critical currents due to HTS tapes volume

Figure 31: Weight of different parameters.

Figure 32: Final weight of different critical currents

It is important that we know that the Synchronous speed will continues for how much time in the motor for this optimized critical current of 60A. In another words we should calculate the time that the persistent currents will be remain in the HTS tapes of the rotor. The leakage inductance of the HTS is constant and equal to 6.77μH

for each phase [9]. The rotor resistance at the below of the critical current (superconducting state) can be calculated with equations bellow:

$$\rho_{HTS} = \frac{E}{j} \tag{40}$$

$$R_{HTS} = \rho_{HTS}\, \frac{L_{HTS}}{a_{HTS}} \tag{41}$$

$$r_r = \frac{1}{3}\, s_r R_{HTS} \tag{42}$$

The calculated rotor resistance in superconducting state is equal to 3.67μΩ. So the time constant in equation (31) is obtained as 1.84s. This short time is sufficient to reach the motor to synchronous speed. For the next times that the persistent current is decreased and accordingly the synchronous torque will be decreased and so the speed will fall down slightly. In this case the motor can increase the torque by inducing current in HTS rotor and reaching its speed to synchronous again and this process will repeat to end.

B. Sensitivity Analysis

For various designers with different valuations (due to their miscellaneous concept from initial judgment results), changes in options can occur. Sensitivity analysis denotes content of algorithm flexibility. As such, the pair-wise comparison matrix of different designs due to various parameters is determined by HTS-ISM designers.

Fig. 33 shows the sensitivity analysis for synchronous torque, starting torque, HTS tapes cooling loss, and HTS tapes volume, from which the Ic=60A is the optimal point for an HTS-ISM. For instance, considering Fig. 34, a new sensitivity analysis is shown so that the weight of starting torque is decreased from 0.55 to 0.37 and the synchronous torque is increased from 0.30 to 0.42. It can be seen that with these new weights, the Ic=80A is the best followed by the Ic=60A. However, the weighting of these parameters depends on designer priority.
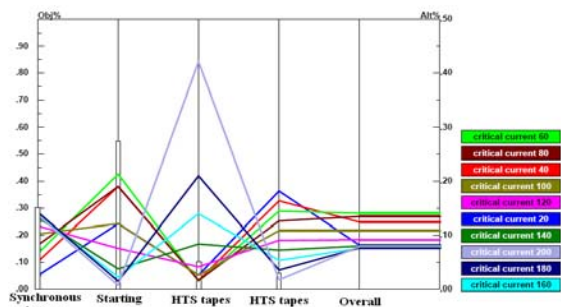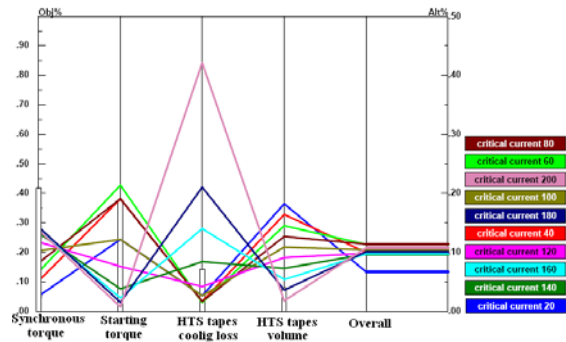

Figure 33: Sensitivity analysis.

Figure 34: Sensitivity analysis with changing of the weights.

9. CONCLUSION

We studied the performance of a squirrel-cage High Temperature Superconducting Induction/ Synchronous Motor (HTS-ISM) based on nonlinear electrical equivalent circuit. The performances of this motor were analyzed by means of the theoretical and numerical methods based on the electrical equivalent circuit. The various specific curves torque versus slip of the HTS-ISM was obtained with numerical methods by changing the critical current of HTS tapes of rotor and it was shown that we can optimize the starting and synchronous torque of the HTS-ISM with changing this critical current. The curves obtained for synchronous and starting torque shown that the variation range of the amount of critical current of HTS tapes of the HTS-ISM considered in this paper can be from 20 A to 200 A. Here, four criteria, synchronous torque, starting torque, HTS tapes cooling loss and HTS tapes volume, according to changes of critical current of the HTS tapes, were analyzed by EC software and were optimized by AHP. It was observed that with changing the weights of any of the criteria related to the ultimate goal depending on designer priority, we can chose the most optimal critical current for HTS tapes of HTS-ISM. Also, for the HTS-ISM considered in this paper, the most optimal critical current was obtained as 60A. This result confirms the critical current of 63A that have been selected by Kyoto University group in the design of the HTS-ISM.

10. REFERENCES

[1] J. Sim, M. Park, H. Lim, G. Cha, J. Ji, and J. Lee, "Test of an induction motor with HTS wire at end ring and bars," IEEE Trans. Applied Superconductivity, vol. 13, no. 2, pp. 2231–2234, 2003.

[2] J. Sim, K. Lee, G. Cha, and J. Lee, "Development of a HTS squirrel cage induction motor with HTS rotor bars," IEEE Trans. Applied Superconductivity, vol. 14, no. 2, pp. 916–919, 2004.

[3] T. Song, and T. Ishigohka, "Experimental study on induction motor with superconducting secondary conductors", IEEE Trans. Applied Superconductivity, vol. 17, no. 2, June 2007

[4] T Nakamura, K Nagao, T Nishimura, Y Ogama, M Kawamoto, T Okazaki, N Ayai and H Oyama, " The direct relationship between output power and current carrying capability of rotor bars in HTS nduction/synchronous motor with the use of DI-BSCCO tapes" , Superconductor Science and Technology, vol. 21, 2008.

[5] T. Nakamura, H. Miyake, Y. Ogama, G. Morita, I. Muta, and T. Hoshino, "Fabrication and characteristics of HTS induction motor by the use of Bi-2223/Ag squirrel cage rotor," IEEE Trans. Applied Superconductivity, vol. 16, no. 2, June 2006

[6] T. Nakamura, Y. Ogama, and H. Miyake, "Performance of inverter fed HTS induction-synchronous motor operated in liquid nitrogen," IEEE Trans. Applied Superconductivity, vol. 17, no. 2, June 2007.

[7] T. Nakamura, Y. Ogama, H. Miyake, K.. Nagao and T. Nishimura, "Novel rotating characteristics of a squirrel-cage-type HTS induction /synchronous motor," Superconductor Science and Technology., vol. 20, pp. 911-918, June 2007.

[8] K. Nagao, T. Nakamura, T. Nishimura, Y. Ogama, N. Kashima, S. Nagaya, K. Suzuki, T. Izumi and Y. Shiohara, "Development and fundamental characteristics of a YBCO superconducting induction/synchronous motor operated in liquid nitrogen" , Superconductor Science and Technology, vol. 21, pp.015022-015026, 2008

[9] G. Morita, T. Nakamura, and I. Muta, "Theoretical analysis of a YBCO squirrel-cage type induction motor based on an equivalent circuit," Superconductor Science and Technology, vol. 19, pp. 473–478, 2006.

[10] T. Nakamura, T. Nishimura, K. Nagao, K. Matsumura and Y. Ogama, "Theoretical analysis of high temperature superconducting induction/synchronous machine based on he nonlinear electrical equivalent circuit", International Conference on Electrical Machines.2008

[11] K. Berger, J. Lévêque, D. Netter, B. Douine, and A. Rezzoug, "Influence of temperature and/or field dependences of the E J power law on trapped magnetic field in bulk YBaCuO," IEEE Trans Applied Superconductivity, vol. 17, no. 2, pp. 3028–3031, june 2007.

[12] N. Schonborg, S. Schonborg and S. Homfelt, "Model of the temperature dependence of the hysteresis losses in a high-temperature superconductor," Physica C, vol. 372-376, pp. 1734-1738, 2002.

[13] Farhad Kazemzadeh and Hossein Heydari "Selecting a best point of Critical Current for the HTS Tapes of an HTS Induction/Synchronous Motor by Analytical Hierarchy Process" 26th international power systam conference, PSC 2011.